Geophysical Research Letters

RESEARCH LETTER
10.1029/2022GL100597

Io Hot Spot Distribution Detected by Juno/JIRAM

F. Zambon[1], A. Mura[1], R. M. C. Lopes[2], J. Rathbun[3], F. Tosi[1], R. Sordini[1], R. Noschese[1], M. Ciarniello[1], A. Cicchetti[1], A. Adriani[1], L. Agostini[4,5], G. Filacchione[1], D. Grassi[1], G. Piccioni[1], C. Plainaki[6], G. Sindoni[6], D. Turrini[7], S. Brooks[2], C. Hansen-Koharcheck[3], and S. Bolton[8]

[1]Istituto Nazionale di AstroFisica—Istituto di Astrofisica e Planetologia Spaziali (INAF-IAPS), Rome, Italy, [2]Jet Propulsion Laboratory, California Institute of Technology, Pasadena, CA, USA, [3]Planetary Science Institute, Tucson, AZ, USA, [4]Centro di Ateneo di Studi e Attività Spaziali (CISAS)"Giuseppe Colombo", Padua, Italy, [5]Istituto Nazionale di AstroFisica—Osservatorio Astronomico di Padova (INAF-OAPd), Padua, Italy, [6]Agenzia Spaziale Italiana, Rome, Italy, [7]Istituto Nazionale di AstroFisica—Osservatorio Astrofisico di Torino (INAF-OATo), Turin, Italy, [8]Southwest Research Institute, San Antonio, TX, USA

Abstract In this work, we present the most updated catalog of Io hot spots based on Juno/JIRAM data. We find 242 hot spots, including 23 previously undetected. Over the half of the new hot spots identified, are located at high northern and southern latitudes (>70°). We observe a latitudinal variability and a larger concentration of hot spots in the polar regions, in particular in the North. The comparison between JIRAM and the most recent Io hot spot catalogs listing power output (Veeder et al., 2015, https://doi.org/10.1016/j.icarus.2014.07.028; de Kleer, de Pater, et al., 2019, https://doi.org/10.3847/1538-3881/ab2380), shows JIRAM detected 63% and 88% of the total number of hot spots, respectively. Furthermore, JIRAM observed 16 of the 34 faint hot spots previously identified. JIRAM data revealed thermal emission from 5 dark pateræ inferred to be active from color ratio images, thus confirming that these are hot spots.

Plain Language Summary We mapped the hot spot distribution on Io's surface by analyzing the images acquired by the JIRAM instrument onboard the Juno spacecraft. We identified 242 hot spots, including 23 not present in other catalogs. A large number of the new hot spots identified are in the polar regions, specifically in the northern hemisphere. The comparison between our work and the most recent and updated catalog reveals that JIRAM detected 82% of the most powerful hot spots previously identified and half of the intermediate-power hot spots, thus showing that these are still active. JIRAM detected 16 out of the 34 faint hot spots previously reported. The resolution of JIRAM may not have been sufficient to detect these faint hot spots, or activity might have faded or stopped.

Key Points:

- We produced a new Io hot spot map based on Juno/JIRAM data
- We identified 242 hot spots, including 23 previously undetected
- The latitudinal hot spot distribution is uneven with a larger concentration at the poles

Supporting Information:

Supporting Information may be found in the online version of this article.

Correspondence to:

F. Zambon,
francesca.zambon@inaf.it

Citation:

Zambon, F., Mura, A., Lopes, R. M. C., Rathbun, J., Tosi, F., Sordini, R., et al. (2023). Io hot spot distribution detected by Juno/JIRAM. *Geophysical Research Letters*, *50*, e2022GL100597. https://doi.org/10.1029/2022GL100597

Received 2 SEP 2022
Accepted 2 DEC 2022
Corrected 31 JAN 2023

This article was corrected on 31 JAN 2023. See the end of the full text for details.

Author Contributions:

Conceptualization: F. Zambon, R. M. C. Lopes, J. Rathbun, F. Tosi
Data curation: F. Zambon, A. Mura, R. Sordini, R. Noschese, A. Cicchetti, L. Agostini
Formal analysis: F. Zambon, A. Mura, R. M. C. Lopes, J. Rathbun, F. Tosi
Funding acquisition: A. Mura
Investigation: F. Zambon, R. M. C. Lopes, J. Rathbun
Methodology: F. Zambon, R. M. C. Lopes, J. Rathbun
Project Administration: A. Mura, S. Bolton
Resources: A. Mura

1. Introduction

Io, the most volcanically active body of our Solar System, displays many volcanic centers, primarily triggered by tidal heating (Peale et al., 1979). The study of Io's volcanic activity is key for understanding the nature of its geological processes, interior and evolution. The distribution of hot spots, as well as their spatial and temporal variability, are extremely important for defining the characteristics of tidal heating, and the mechanisms by which heat escapes from the interior (e.g., Davies et al., 2015; de Kleer, de Pater, et al., 2019; Hamilton et al., 2013; Lopes et al., 1999; Rathbun et al., 2014; Tackley, 2013; Tackley et al., 2001).

The distribution of volcanoes on Io could discriminate between different interior models, which predict greater activity concentrated at low latitudes due to a more ductile lithosphere, or vice versa an activity distributed homogeneously on a global scale, favored by a "magma ocean" that mechanically decouples the lithosphere from the deeper interior (de Kleer, McEwen, & Park, 2019). In this regard, the polar perspective from which the Juno/Jovian InfraRed Auroral Mapper (JIRAM, Adriani et al., 2017) can observe Io is extremely complementary to Earth-based observations, and can significantly contribute to the effort made over the years to shed light on this aspect.

Io has been studied for decades by ground-based and remote sensing observations (e.g., Davies et al., 2015; de Kleer, de Pater et al., 2019; de Pater et al., 2017; de Kleer et al., 2021; Mura et al., 2020; Lopes and Williams, 2005; Rathbun et al., 2014). The first evidence of volcanism on Io dates back to the first high-resolution images of the Jupiter system returned by the NASA Voyager 1 mission in 1979 (Morabito et al., 1979; Smith et al., 1979). Io

Software: F. Zambon, A. Mura
Supervision: F. Zambon, A. Mura, R. M. C. Lopes, J. Rathbun
Validation: F. Zambon
Visualization: F. Zambon, A. Mura, R. M. C. Lopes, J. Rathbun, F. Tosi
Writing – original draft: F. Zambon
Writing – review & editing: F. Zambon, A. Mura, R. M. C. Lopes, J. Rathbun, F. Tosi, R. Noschese, M. Ciarniello, A. Adriani, L. Agostini, G. Filacchione, D. Grassi, G. Piccioni, C. Plainaki, G. Sindoni, D. Turrini, S. Brooks, C. Hansen-Koharcheck, S. Bolton

was later observed in much greater detail by the NASA Galileo mission in the period 1996–2003 (Lopes-Gautier et al., 1999; McEwen et al., 2000), and was observed from a large distance by the NASA-ESA-ASI Cassini Orbiter (2000) on its way to Saturn (Radebaugh et al., 2004). In 2007, the NASA New Horizons spacecraft also acquired images of Io, highlighting the eruption of the volcano Tvashtar (Spencer et al., 2007).

In recent years, the Juno spacecraft observed Io during several orbits, and is still acquiring data at the time of writing. Mura et al. (2020) reported on preliminary mapping of Io from JIRAM, identifying 48 hot spots. Juno is the first mission entirely dedicated to Jupiter and its satellite system after NASA's Galileo and, thanks to its observational strategy, JIRAM is able to get a more direct look at Io's poles, poorly observed before.

Several catalogs of Io's volcanic centers have been published before, summarizing hot spots detected on the basis of remote sensing (Lopes & Spencer, 2007; Mura et al., 2020; Rathbun et al., 2004; Veeder et al., 2015) and ground-based observations (e.g., Cantrall et al., 2018; de Kleer, de Pater, et al., 2019; de Pater et al., 2004; de Kleer and de Pater 2016a, 2016b). In particular, Veeder et al. (2015) updated the Io hot spots detected by other authors (e.g., de Pater et al., 2004; Lopes-Gautier et al., 1999; Lopes and Spencer, 2007; Rathbun et al., 2004; Spencer, McEwen, et al., 1997; Spencer, Stansberry, et al., 1997; Veeder et al., 2015), producing the most up-to-date global heat flow map of the Io volcanic thermal sources, collecting 243 hot spots and including new detection based on the Galileo/NIMS data.

Here, we show the latest map of Io hot spots based on JIRAM infrared images. In particular, we analyzed the distribution of hot spots by comparing our results with previous findings, with the goal of analyzing their spatial distribution on Io's surface.

2. Data Set and Methods

We analyze data acquired by JIRAM, the spectro-imager onboard Juno mainly devoted to the study of Jupiter's atmosphere. During its journey around Jupiter, JIRAM has also had the opportunity to acquire a large amount of data on the Galilean satellites, improving our knowledge of these bodies.

JIRAM is equipped with a slit spectrometer covering the wavelength range between 2 and 5 μm and an imager with the two L-band and M-band filters, centered at 3.45 and 4.78 μm, respectively. The slit spectrometer is co-located within the M-band imager's field of view, sharing the same telescope (Adriani et al., 2017).

Here, we used JIRAM M-band images from the Juno orbits: 10, 11, 16, 17, 18, 20, 24, 25, 26, 27, 32, 33, those currently available, with a spatial resolution ranging from 48 to 154 km/pixel. We excluded data from the early Juno orbits, characterized by coarser spatial resolution and already discussed in Mura et al. (2020).

For each orbit, we consider a set of images called "super images," obtained by averaging multiple JIRAM observations acquired over a timeframe of a few minutes. This approach minimizes the effects due to spurious pixels induced by radiation noise, reducing the possibility of false positives. Figure 1 shows a representative subset of super images for each orbit. For each pixel within a given super image, we calculated the most relevant geometric information, that is, planetocentric latitude, planetocentric longitude, solar incidence angle, and emission angle. In Table S1 in Supporting Information S1, we report all the JIRAM super images considered for this work, along with their main characteristics and grouped by orbit.

JIRAM data have good spatial resolution and coverage, including the polar regions, which were poorly investigated by past spacecraft and ground-based observations. Across the different orbits, the JIRAM sub-spacecraft latitude varies between ∼−78° and ∼57° (Figure S1 and Table S1 in Supporting Information S1). The high northern and southern sub-S/C latitudes reached by JIRAM improved the coverage of Io's polar regions, allowing us to better investigate areas poorly covered by previous observations.

Figures S1 and S2 in Supporting Information S1 show that the JIRAM global coverage of Io is uneven. The equatorial and northern regions have larger redundancy with respect to the southern areas, reaching an overlap up to 43 super images per pixel. A small region at around 215°–268°W and 60°–15°S is not covered by any JIRAM observation.

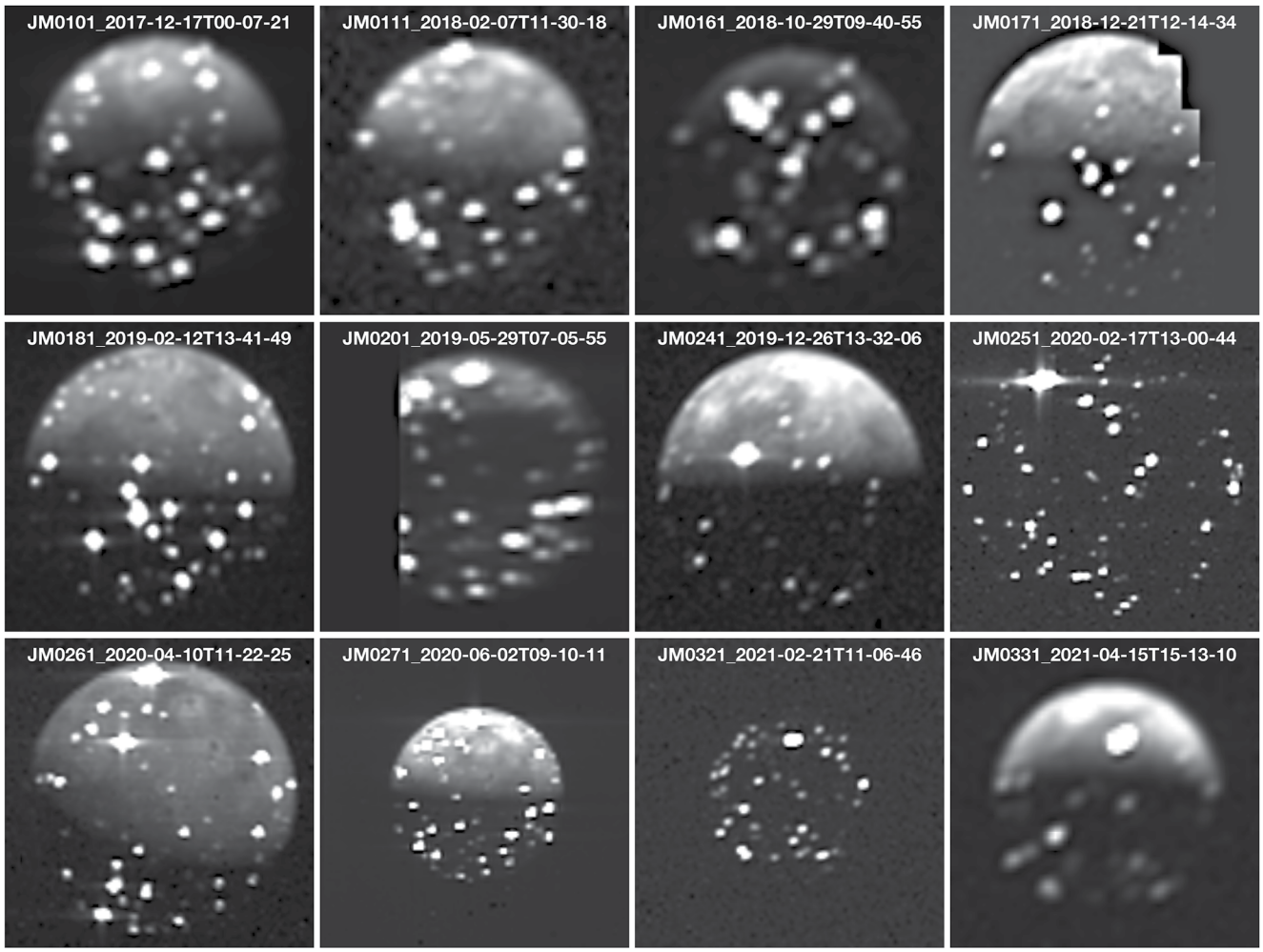

Figure 1. Examples of Io representative subset of JIRAM M filter "super images" for each orbit. The super images have been obtained averaging contiguous JIRAM acquisitions.

To identify Io hot spots, we applied the following steps:

1. We filtered the super images ruling out those pixels with emission angles >75°, to limit uncertainties due to limb proximity.
2. The images have been acquired at different solar incidence angles, thus Io images can cover the dayside, the nightside or can be in eclipse (see Figure 1). Due to the higher background terrain radiance, the identification of hot spots on the dayside or close to the Sun terminator was challenging with respect to the nightside or eclipse cases. To overcome this problem, we divided the images into three categories: dayside ($i \leq 70°$), dawn/dusk ($70° < i < 90°$) and nightside $i \geq 90°$.
3. For each super image, we selected as background the areas without any hot spot evidence, and we calculated the median value of the radiance for the dayside, nightside and dawn/dusk background. Hence, we consider as hot spot detection threshold those radiance values strictly larger than the median radiance for the nightside, while we found an average of 0.003 W/m^2sr^{-1} is adequate to discriminate between hot spot and background in dawn/dusk and on the dayside. Eventually, we evaluate the radiance values of each hot spots automatically selected to avoid false detection.
4. We produced a global radiance map, including all JIRAM orbits, and a global radiance map for each orbit, averaging overlapping data. Since the best spatial resolution achieved by JIRAM in our data set is 48 km, which on a great circle of the surface of Io corresponds to 1.5°, angular bins of 1.5° × 1.5° are adequate to present our JIRAM data. For this reason, we consider a grid with fixed angular bins of 1.5° both in latitude

and longitude. Radiance maps for each orbit (see Figure S3 in Supporting Information S1) clearly show the hot spot distribution and the JIRAM coverage of Io's surface.

5. We selected hot spots from the global radiance maps for each orbit and we calculated the central latitude and longitude for each hot spot, which is reported in Table S2 in Supporting Information S1. Many hot spots are observed in several super images acquired at different orbits and under different illumination conditions. On the dayside, a photometric model is needed to correct the portion of reflected solar radiation, which at 4.8 μm is not negligible, especially far from the terminator. It is not necessary to photometrically correct each hot spot individually, but rather the whole dayside to separate the thermal emission from the reflected part. Since no robust photometric model is yet available for Io in the 4.6–5.0 μm spectral range covered by the JIRAM M-band filter, we do not report the radiance values and we defer to future works for the study of the hot spots' temporal variability.
6. We double-checked the hot spots found from the super images with those of the radiance maps to avoid any duplication.
7. To identify known and previously undetected hot spots, we calculated the angular separation between the position in our catalog and that reported by previous literature (e.g., Cantrall et al., 2018; de Kleer, de Pater, et al., 2019; Lopes and Spencer, 2007; Mura et al., 2020; Veeder et al., 2015). Hot spots very close to previous detections (distance $\leq 3°$) are identified as known hot spots. Those that lie within an angular distance ranging from 3° to 6° are flagged as "uncertain," while we consider as safe previously undetected those hot spots that show up at an angular distance $\geq 6°$ compared to all previous detections. Since most Io pateræ can reach 150 km in size, an angular distance of 3°–6° is adequate to separate different hot spots including a margin of uncertainty.
8. Finally, we built a GIS shapefile including all of the hot spots. For each hot spot, we indicate the planetocentric coordinates, we assign an identification number, we associate an official name when available, we indicate the Juno orbits in which the hot spots was observed, we include literature references, and we put additional information and whether the hot spots had been previously detected (see Table S2 in Supporting Information S1).

3. Io Hot Spot Distribution as Observed by JIRAM

Here we present the distribution of Io hot spots detected by JIRAM, improving the work initiated by Mura et al. (2020). We identified 242 hot spots distributed across the entire satellite. Figure 2a shows their global distribution on Io's surface. We indicated in blue those hot spots already present in other catalogs, in orange the uncertain ones, and in green those we consider as previously undetected hot spots. Table S2 in Supporting Information S1 reports all the details for each hot spot.

Io's hot spots can vary greatly in their degree of activity (e.g., Davies et al., 2012a, 2012b; Lopes et al., 2004; Rathbun et al., 2002). As such, we do not expect JIRAM to detect every previously identified hot spot, even if the global coverage was complete. We have compared the distribution of JIRAM hot spots with the most up-to-date catalogs available from spacecraft and ground-based observations, in particular: Lopes and Spencer (2007), Veeder et al. (2015), Cantrall et al. (2018), de Kleer, de Pater et al. (2019), and Mura et al. (2020).

Lopes and Spencer (2007) listed hot spots detected by Galileo, Voyager, and ground-based observations up to that date. After 2007, various papers listed hot spots detected from ground-based Adaptive Optics observations (e.g., Cantrall et al., 2018; de Kleer et al., 2014), from New Horizons (Spencer et al., 2007; Tsang et al., 2014) and from JIRAM during the initial orbits of Juno (Mura et al., 2020). In addition, Veeder et al. (2015) (Table 2) listed hot spots detected up to that date and also the power output from 24 small "dark pateræ" from where thermal emission had not been detected, but was inferred using color ratio images. JIRAM was able to detected thermal emission from five of these, thus confirming that these are hot spots.

Lopes and Spencer (2007) and Veeder et al. (2015) are the most extensive hot spot catalogs, and they list 212 and 243 hot spots, covering a latitude range between −72.3° and 81.6° and −80.5° and 83.4°, respectively. The other catalogs considered in this work show a smaller number of detection, reaching up to latitude values between −70.8 and 81.6°. The high sub S/C latitude values achieved by JIRAM (see Figure S1 and Table S1 in Supporting Information S1), improved significantly the coverage of the polar areas, catching up the latitude spanning between −85.1° and 83.6°. Histograms in Figure 3a show the latitudinal distribution of JIRAM hot spots compared with the other catalogs considered here, while Figure 3c reports the number of hot spots detected by JIRAM for each latitudinal bin (1.5°). The northern hemisphere contains a larger number of hot spots than

10.1029/2022GL100597

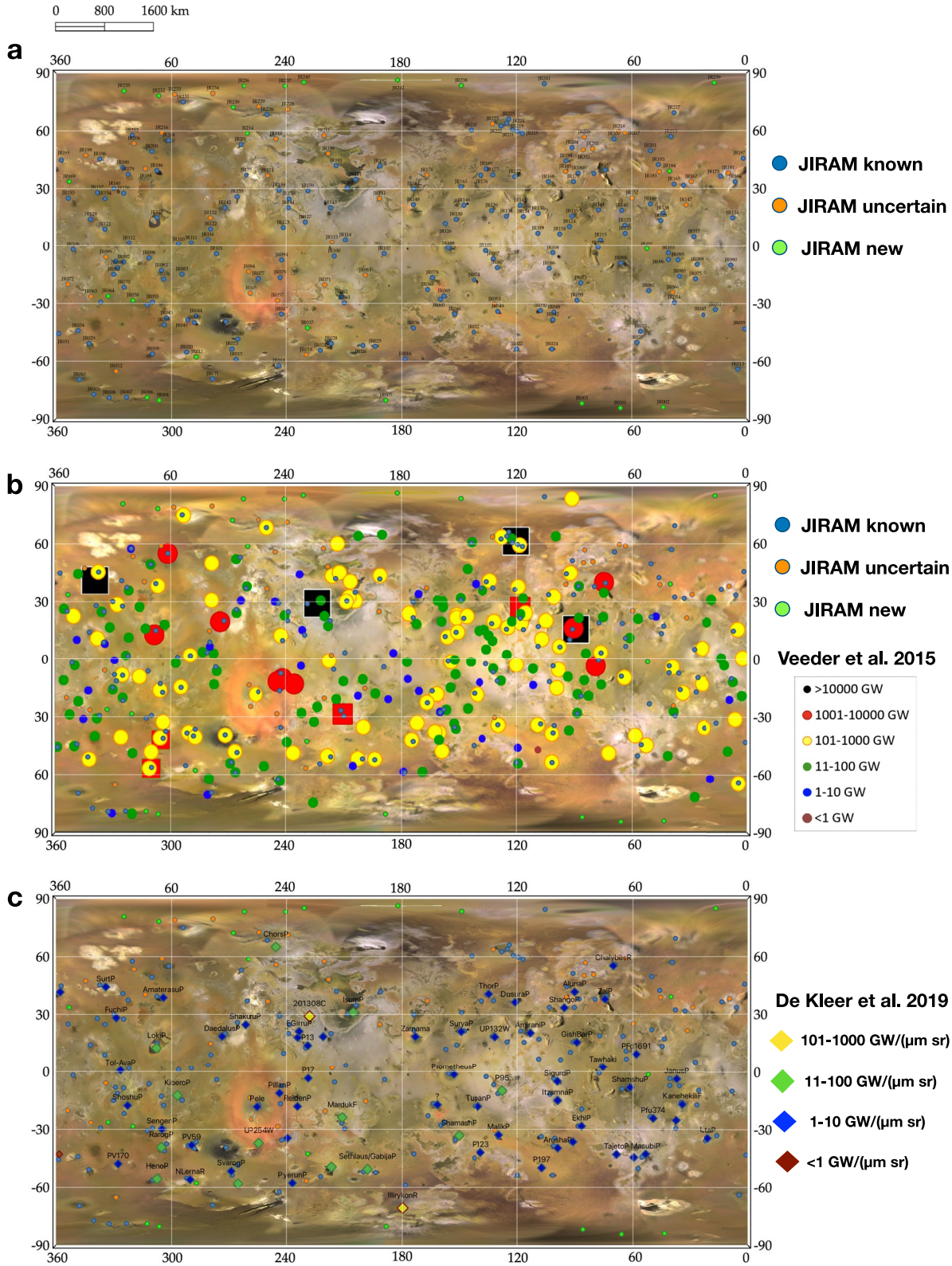

Figure 2.

the southern one, 133 versus 109 hot spots. The ratio between the number of hot spots for latitude larger than 70°N and lower than 70°S is ∼1.7. In particular, the northern polar region contains 6.2% of the total number of detection, while the southern 3.7%. This could indicate an asymmetry in the volcanic activity on Io. However, we must consider the smaller coverage and coarser spatial resolution of the southern region compared to northern latitudes, which could affect our interpretation (see the Figures S1 and S3 in Supporting Information S1). At first glance, it appears that most hot spots are concentrated in the mid-latitude region (−50°, +50°), while in the polar regions we identified a smaller number of hot spots (Figure 3c). Nevertheless, after correcting for the surface area in each latitude bin, we find a larger concentration of hot spots in the polar regions rather than in the equatorial area (Figure 3d). This result is emphasized in Figure 3e, where we show the JIRAM latitudinal hot spot density compared with those found by other authors.

In Figure 3f, we plot the number of hot spots for northern and southern latitudes >70°. The better coverage achieved by JIRAM at high latitudes is reflected in the major concentration of hot spots at the poles compared to other catalogs (Cantrall et al., 2018; de Kleer, de Pater, et al., 2019; Mura et al., 2020; Lopes & Spencer, 2007; Veeder et al., 2015). The number of hot spots we detected in the high latitude regions is over double with respect to those found in the other catalogs.

The longitudinal hot spot variation does not highlight major differences between the trailing and leading hemisphere (see histograms in Figure 3b). The number of hot spots in the trailing hemisphere (126) is slightly larger than in the leading hemisphere (116). The ratio between the number of hot spots in the leading and trailing hemisphere is 0.92, corresponding to a percent of hot spots of 0.48% and 0.52% of the total, for the leading and trailing hemisphere, respectively.

We observed a reduction in the number of hot spots around 180°W and 0°, which is likely due to poor JIRAM coverage in those areas (see Figure S2 in Supporting Information S1).

Most of the hot spots we identified (219) have been already detected by other authors or are flagged as uncertain detections (e.g., Appendix 1 in Lopes and Spencer (2007); Cantrall et al., 2018; de Kleer, de Pater, et al., 2019; Mura et al., 2020; Veeder et al., 2015), while 23 are previously undetected as they do not show up in any other catalog. Over half of the 23 new hot spots are located in the polar regions (latitude >70°) (Figure 2a). These detections are mainly due to the Juno mission profile, and its polar orbit, as previously stated.

In Figure 2b, we compare the hot spot distribution obtained by JIRAM with those of Veeder et al. (2015), where hot spots are grouped by heat flow power. They calculated the power output after retrieving the effective temperature fitting radiance flux from the one- and two-temperature models described by Davies et al. (1997, 2001) and Davies (2003, 2007) by using the Galileo/NIMS corrected data.

We identified 63% of the overall hot spots detected by Veeder et al. (2015). Comparing the distribution of our data with the Io global heat flow power hot spot map by Veeder et al. (2015), we observed that the highest power heat flow hot spots (>1000 GW), except Reiden, are still visible in JIRAM data, and represent the major volcanic centers (e.g., Loki, Pillan, Dazhbog, Daedalus, Marduk, Zal, and Gish Bar). We did not detect Reiden Patera from JIRAM images, but it was identified by Galileo's SSI imager in 1996 during an observation obtained in eclipse. After that, it was not detected again until 1999–2001 (Lopes & Spencer, 2007).

We found some differences between high heat flow power (101–1000 GW) detected by Veeder et al. (2015) and our map. We detected ∼82% of the high power hot spots, and only 16 of the 89 identified by Veeder et al. (2015) with this power heat flow are not in our list (such as Ruwa, Emakong, Aten, etc.).

The largest discrepancies involve hot spots with low power heat flow (11–100 GW). Out of the 111 hot spots listed by Veeder et al. (2015), including 11 "dark pateræ," with power output between 11 and 100 GW, JIRAM detected 56, 2 of which are listed as "dark pateræ," confirming that these two are hot spots.

Figure 2. (a) Io hot spot map derived by Juno/JIRAM super images. Blue circles indicate the hot spots observed by JIRAM, and already present in other catalogs. Orange circles show the uncertain previously undetected hot spots, while green circles represent the previously undetected hot spots observed by JIRAM. (b) JIRAM hot spot distribution compared with those observed by Veeder et al. (2015) derived by Galileo/NIMS data. Different colors correspond with various power output range of values as reported in the legend. Black squares represent very high power outbursts not persistent hot spots. Image adapted from Veeder et al. (2015). (c) JIRAM detection compared with those of de Kleer, de Pater et al. (2019), derived from Keck and Gemini N telescopes. We considered the hot spots listed in de Kleer, de Pater et al. (2019) (Table 1). The mean observed flux density is retrieved by L_p (3.78 μm) data, if no data were available in that filter, they considered the M_s filter (4.67 μm) data. If no L_p and M_s were present they selected narrowband filter images.

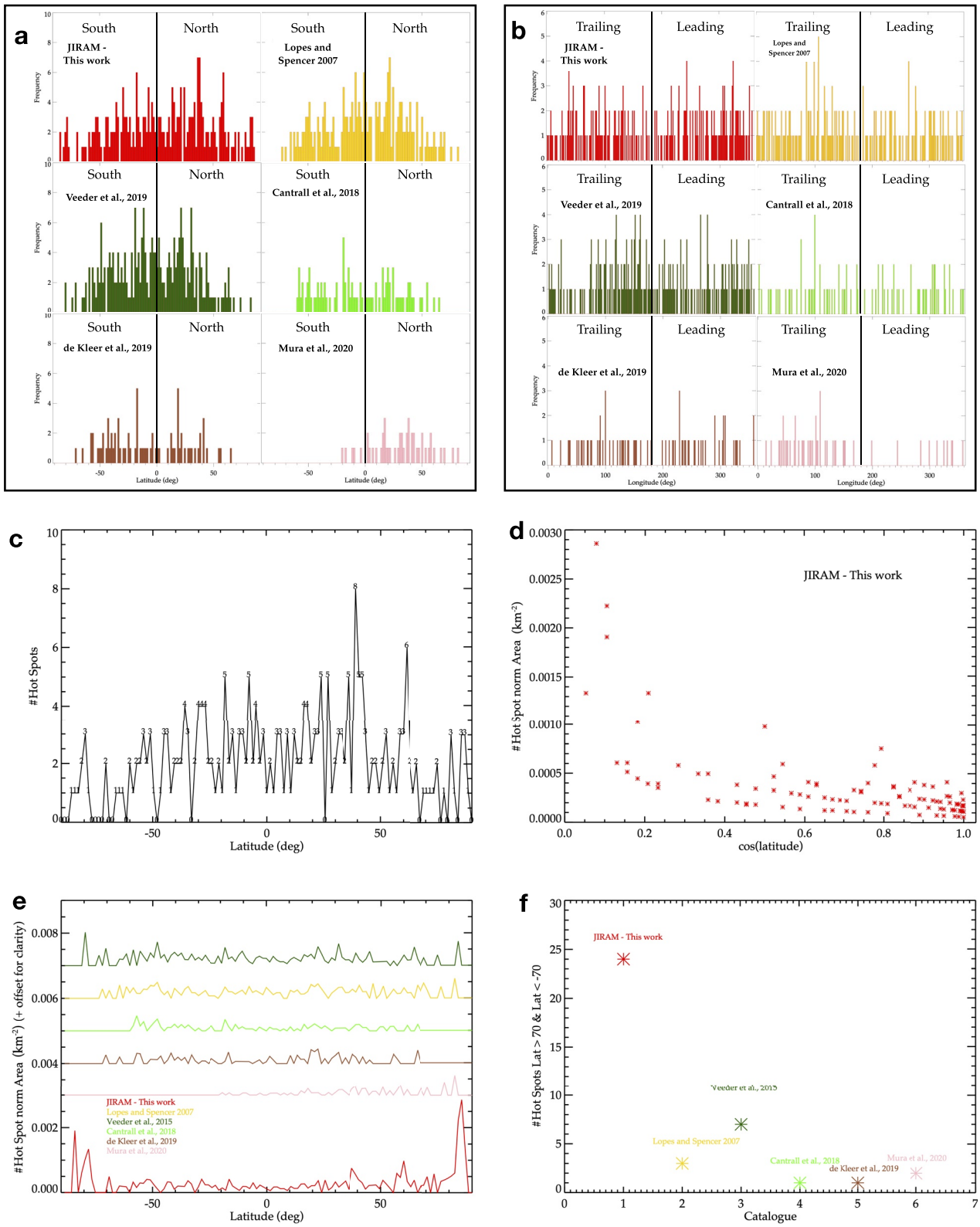

Figure 3. JIRAM Io hot spot latitudinal (a) and longitudinal (b) distribution (in red), compared with other catalogs indicated with different color. (c) Number of JIRAM hot spots enclosed in latitudinal bins of 1.5°. (d) Number of JIRAM hot spots normalized by latitudinal bin area versus cosine of the latitude. (e) Hot spot latitudinal distribution normalized for area enclosed in each bin (1.5°) for different catalogs compared with JIRAM results (red curve). (e) Number of hot spots for northern and southern latitudes >70°.

Among the 34 faint hot spots listed by Veeder et al. (2015) with power output ≤10 GW, JIRAM detected 16. Out of the 18 not detected by JIRAM, 12 were listed by Veeder et al. (2015) as "dark pateræ," from where no thermal emission had been previously detected by NIMS. JIRAM was able to detect thermal emission from three of these faint "dark pateræ," also confirming that these are hot spots.

de Kleer, de Pater et al. (2019) reported detection from time domain adaptive optics observations between 2013 and 2018. They analyzed the flux density of 75 volcanic centers, studying their temporal variability. To derive the mean observed flux density, they used the Keck and Gemini N telescopes data. In particular, they considered the L_p filter data centered at 3.78 μ. If no L_p observations were available, they select M_s filter data centered at 4.67 μm, while they compensate for the lack of L_p and M_s images with the narrowband filter images.

Figure 2c shows JIRAM detection compared with those of de Kleer, de Pater et al. (2019). We identified ∼88% of the hot spots listed by de Kleer, de Pater et al. (2019). A large part of these hot spots (∼75%) is characterized by flux density between 1 and 10 GWμm^{-1}sr^{-1}, and only 7 have not been observed by JIRAM, while 12 of the 13 hot spots with flux density ranging between 11 and 101 GWμm^{-1}sr^{-1} are present in our database. Only 2 hot spots have a flux density >101 GWμm^{-1}sr^{-1}.

This is not surprising, as the surface of Io is very dynamic. It is possible that the weaker volcanic centers were either not active at the time of JIRAM observations, or their activity was too weak to be detected. The brightest eruptive centers appear to be persistent at least over decades.

However, we note that the different spatial resolution coverage and the integration time play a key role in the ability of identifying Io hot spots. For this reason, new JIRAM high resolution observations are fundamental to better characterize Io hot spot distribution and variability especially in regions with a poor coverage.

4. Conclusions

In this paper, we mapped the Io hot spot distribution by using Juno/JIRAM data M-band (4.8 μm) optical imagery to obtain "super images" from orbits: 10, 11, 16, 17, 18, 20, 24, 25, 26, 27, 32, and 33, with a spatial resolution ranging from 48 to 154 km/pixel. Below, we summarize the results obtained:

- We identified 242 hot spots. The longitudinal distribution indicates no significant difference between the leading and trailing hemispheres. However, the latitudinal distribution, normalized by area, indicates a larger concentration of hot spots in the polar regions compared to the intermediate latitudes. We also observed a larger concentration of hot spots in the northern polar region compared to the southern one. This may indicate differences in internal dynamics. Even though, at present JIRAM's coverage of the northern hemisphere is larger and has higher spatial resolution than the southern region.
- We compare our results with those of the literature (e.g., Cantrall et al., 2018; de Kleer, de Pater, et al., 2019; Lopes and Spencer, 2007; Mura et al., 2020; Veeder et al., 2015). We detected 23 previously undetected hot spots, over half of which located in the polar regions. This is expected since the polar regions were poorly observed before Juno. The discovery of previously undetected hot spots will be useful to better constrain tidal dissipation models which are predicted to result in surface patterns of heat flow and, likely, hot spot distribution characteristic of that model (e.g., Ross et al., 1990; Tackley, 2013; Tackley et al., 2001). Current data at a global scale (∼40–100 km/pixel) (de Kleer & de Pater, 2016b; Mura et al., 2020; Rathbun et al., 2018), have not unambiguously distinguished between different interior models. Future JIRAM observations will significantly improve the spatial resolution up to at least 20 km/pixel, permitting a more accurate Io hot spot detection.
- We detected ∼88% of the 75 hot spots reported by de Kleer, de Pater, et al. (2019). We found large discrepancies (7 hot spots) with the low density flux (<10 GWμm^{-1}sr^{-1}) hot spots, while we do not identified only two of the hot spots with larger density flux (<100 GWμm^{-1}sr^{-1}).
- With one exception, we detected all of the most powerful hot spots (>1000 GW) previously reported by Veeder et al. (2015), confirming previous suggestions that some of Io's hot spots may be active over decades or more (e.g., de Kleer, de Pater, et al., 2019). We also detected 82% of the hot spots with heat flow power ranging between 101 and 1000 GW, 16 out of the 89 hot spots listed by Veeder et al. (2015). We did not detect half of the faint hot spots (<100 GW) reported by Veeder et al. (2015) and found that this major discrepancy lies in the weak (or lower-power) hot spots. One possibility is that these hot spots were not active at the time JIRAM observed.

Alternatively, those weak hot spots may still be active but their power is below the JIRAM detection threshold. On the other hand, the catalogs considered here, are based on data acquired at various wavelengths by different instruments, influencing the hot spot detection and their heat flow power and temperature retrieval.

The Io hot spot map presented in our work is the most updated among those based on remote sensing datasets. JIRAM Io observations are still ongoing, and future higher spatial resolution images will be fundamental to extend and confirm our results, to better highlight weak hot spots and to improve our overall knowledge of Io volcanic processes and evolution.

Data Availability Statement

JIRAM data used in this paper are publicly available in the Planetary Data System (PDS) at the following link: https://atmos.nmsu.edu/PDS/data/PDS4/juno_jiram_bundle/data_raw/. The Juno/JIRAM Io hot spot map shown in this paper is available as GIS shapefile at the following Zenodo link: Zambon (2022).

Acknowledgments
This work is supported by the Agenzia Spaziale Italiana (ASI). JIRAM is funded by the ASI-INAF agreement no. 2016-23-H.0. Part of this work was performed at the Jet Propulsion Laboratory, California Institute of Technology, under contract with NASA.

References

Adriani, A., Filacchione, G., Di Iorio, T., Turrini, D., Noschese, R., Cicchetti, A., et al. (2017). JIRAM, the Jovian infrared auroral mapper. *Space Science Reviews*, *213*(1–4), 393–446. https://doi.org/10.1007/s11214-014-0094-y

Cantrall, C., de Kleer, K., de Pater, I., Williams, D. A., Davies, A. G., & Nelson, D. (2018). Variability and geologic associations of volcanic activity on Io in 2001-2016. *Icarus*, *312*, 267–294. https://doi.org/10.1016/j.icarus.2018.04.007

Davies, A. G. (2003). Volcanism on Io: Estimation of eruption parameters from Galileo NIMS data. *Journal of Geophysical Research*, *108*(E9), 5106–5120. https://doi.org/10.1029/2001JE001509

Davies, A. G. (2007). *Volcanism on Io: A comparison with Earth*. Cambridge University Press.

Davies, A. G., Keszthelyi, L. P., Williams, D. A., Phillips, C. B., McEwen, A. S., Lopes, R. M. C., et al. (2001). Thermal signature, eruption style and eruption evolution at Pele and Pillan on Io. *Journal of Geophysical Research*, *106*(E12), 33079–33104. https://doi.org/10.1029/2000JE001357

Davies, A. G., McEwen, A. S., Lopes-Gautier, R., Keszthelyi, L., Carlson, R. W., & Smythe, W. D. (1997). Temperature and area constraints of the South Volund volcano on Io from the NIMS and SSI instruments during the Galileo G1 orbit. *Geophysical Research Letters*, *24*(20), 2447–2450. https://doi.org/10.1029/97GL02310

Davies, A. G., Veeder, G. J., Matson, D. L., & Johnson, T. V. (2012a). Charting thermal emission variability at Pele, Janus Patera and Kanehekili Fluctus with the Galileo NIMS Io thermal emission database (NITED). *Icarus*, *221*(1), 466–470. https://doi.org/10.1016/j.icarus.2012.04.012

Davies, A. G., Veeder, G. J., Matson, D. L., & Johnson, T. V. (2012b). Io: Charting thermal emission variability with the Galileo NIMS Io thermal emission database (NITED): Loki Patera. *Geophysical Research Letters*, *39*(1), L01201. https://doi.org/10.1029/2011GL049999

Davies, A. G., Veeder, G. J., Matson, D. L., & Johnson, T. V. (2015). Map of Io's volcanic heat flow. *Icarus*, *262*, 67–78. https://doi.org/10.1016/j.icarus.2015.08.003

de Kleer, K., & de Pater, I. (2016a). Spatial distribution of Io's volcanic activity from near-IR adaptive optics observations on 100 nights in 2013-2015. *Icarus*, *280*, 405–414. https://doi.org/10.1016/j.icarus.2016.06.018

de Kleer, K., & de Pater, I. (2016b). Time variability of Io's volcanic activity from near-IR adaptive optics observations on 100 nights in 2013-2015. *Icarus*, *280*, 378–404. https://doi.org/10.1016/j.icarus.2016.06.019

de Kleer, K., de Pater, I., Davies, A. G., & Ádámkovics, M. (2014). Near-infrared monitoring of Io and detection of a violent outburst on 29 August 2013. *Icarus*, *242*, 352–364. https://doi.org/10.1016/j.icarus.2014.06.006

de Kleer, K., de Pater, I., Molter, E. M., Banks, E., Davies, A. G., Alvarez, C., et al. (2019). Io's volcanic activity from time domain adaptive optics observations: 2013-2018. *The Astronomical Journal*, *158*(1), 29. https://doi.org/10.3847/1538-3881/ab2380

de Kleer, K., McEwen, A., & Park, R. (2019). *Tidal heating: Lessons from Io and the Jovian system*. Final Report for the Keck Institute for Space Studies. Retrieved from https://kiss.caltech.edu/final_reports/Tidal_Heating_final_report.pdf

de Kleer, K., Skrutskie, M., Leisenring, J., Davies, A. G., Conrad, A., de Pater, I., et al. (2021). Resolving Io's volcanoes from a mutual event observation at the large binocular telescope. *Planetary Science Journal*, *2*(6), 227. https://doi.org/10.3847/PSJ/ac28fe

de Pater, I., de Kleer, K., Davies, A. G., & Ádámkovics, M. (2017). Three decades of Loki Patera observations. *Icarus*, *297*, 265–281. https://doi.org/10.1016/j.icarus.2017.03.016

de Pater, I., Marchis, F., Macintosh, B. A., Roe, H. G., Le Mignant, D., Graham, J. R., & Davies, A. G. (2004). Keck AO observations of Io in and out of eclipse. *Icarus*, *169*(1), 250–263. https://doi.org/10.1016/j.icarus.2003.08.025

Hamilton, C. W., Beggan, C. D., Still, S., Beuthe, M., Lopes, R. M. C., Williams, D. A., et al. (2013). Spatial distribution of volcanoes on Io: Implications for tidal heating and magma ascent. *Earth and Planetary Science Letters*, *361*, 272–286. https://doi.org/10.1016/j.epsl.2012.10.032

Lopes, R., Fagents, S., Mitchell, K. T., & Gregg, T. (1999). *Modeling volcanic processes: The physics and mathematics of volcanism* (pp. 384–413). Cambridge University Press. https://doi.org/10.1017/CBO9781139021562.017

Lopes, R., & Spencer, J. R. (2007). *Io after Galileo: A new view of Jupiter's volcanic Moon*. Springer.

Lopes, R., & Williams, D. A. (2005). Io after Galileo. *Reports on Progress in Physics*, *68*(2), 303–340. https://doi.org/10.1088/0034-4885/68/2/R02

Lopes, R. M. C., Kamp, L. W., Smythe, W. D., Mouginis-Mark, P., Kargel, J., SSI Teams, et al. (2004). Lava lakes on Io: Observations of Io's volcanic activity from Galileo NIMS during the 2001 fly-bys. *Icarus*, *169*(1), 140–174. https://doi.org/10.1016/j.icarus.2003.11.013

Lopes-Gautier, R., McEwen, A. S., Smythe, W. B., Geissler, P. E., Kamp, L., SSI Teams, et al. (1999). Active volcanism on Io: Global distribution and variations in activity. *Icarus*, *140*(2), 243–264. https://doi.org/10.1006/icar.1999.6129

McEwen, A. S., Belton, M. J. S., Breneman, H. H., Fagents, S. A., Geissler, P., Greeley, R., et al. (2000). Galileo at Io: Results from high-resolution imaging. *Science*, *288*(5469), 1193–1198. https://doi.org/10.1126/science.288.5469.1193

Morabito, L. A., Synnott, S. P., Kupferman, P. N., & Collins, S. A. (1979). Discovery of currently active extraterrestrial volcanism. *Science*, *204*(4396), 972. https://doi.org/10.1126/science.204.4396.972

Mura, A., Adriani, A., Tosi, F., Lopes, R. M. C., Sindoni, G., Filacchione, G., et al. (2020). Infrared observations of Io from Juno. *Icarus*, *341*, 113607. https://doi.org/10.1016/j.icarus.2019.113607

Peale, S. J., Cassenand, P., & Reynolds, R. T. (1979). Infrared observations of the Jovian system from voyager 1. *Science*, *203*(4383), 892–894. https://doi.org/10.1126/science.203.4383.892

Radebaugh, J., McEwen, A. S., Milazzo, M. P., Keszthelyi, L. P., Davies, A. G., Turtle, E. P., & Dawson, D. D. (2004). Observations and temperatures of Io's Pele Patera from Cassini and Galileo spacecraft images. *Icarus*, *169*(1), 65–79. https://doi.org/10.1016/j.icarus.2003.10.019

Rathbun, J. A., Lopes, R. M. C., & Spencer, J. R. (2018). The global distribution of active ionian volcanoes and implications for tidal heating models. *The Astronomical Journal*, *156*(5), 11. https://doi.org/10.3847/1538-3881/aae370

Rathbun, J. A., Spencer, J. R., Davies, A. G., Howell, R. R., & Wilson, L. (2002). Loki, Io: A periodic volcano. *Geophysical Research Letters*, *29*(10), 84-1–84-4. https://doi.org/10.1029/2002GL014747

Rathbun, J. A., Spencer, J. R., Lopes, R. M., & Howell, R. R. (2014). Io's active volcanoes during the new Horizons era: Insights from new Horizons imaging. *Icarus*, *231*, 261–272. https://doi.org/10.1016/j.icarus.2013.12.002

Rathbun, J. A., Spencer, J. R., Tamppari, L. K., Martin, T. Z., Barnard, L., & Travis, L. D. (2004). Mapping of Io's thermal radiation by the Galileo photopolarimeter-radiometer (PPR) instrument. *Icarus*, *169*(1), 127–139. https://doi.org/10.1016/j.icarus.2003.12.021

Ross, M. N., Schubert, G., Spohn, T., & Gaskell, R. W. (1990). Internal structure of Io and the global distribution of its topography. *Icarus*, *85*(2), 309–325. https://doi.org/10.1016/0019-1035(90)90119-T

Smith, B. A., Shoemaker, E. M., Kieffer, S. W., & Cook, A. F. (1979). The role of SO2 in volcanism on Io. *Natur*e, *280*(5725), 738–743. https://doi.org/10.1038/280738a0

Spencer, J. R., McEwen, A. S., McGrath, M. A., Sartoretti, P., Nash, D. B., Noll, K. S., & Gilmore, D. (1997). Volcanic resurfacing of Io: Post-repair HST imaging. *Icarus*, *127*(1), 221–237. https://doi.org/10.1006/icar.1996.5670

Spencer, J. R., Stansberry, J. A., Dumas, C., Vakil, D., Pregler, R., Hicks, M., & Hege, K. (1997). A history of high-temperature Io volcanism: February 1995 to May 1997. *Geophysical Research Letters*, *24*(20), 2451–2454. https://doi.org/10.1029/97GL02591

Spencer, J. R., Stern, S. A., Cheng, A. F., Weaver, H. A., Reuter, D. C., Retherford, K., et al. (2007). Io volcanism seen by new Horizons: A major eruption of the Tvashtar volcano. *Science*, *318*(5848), 240–243. https://doi.org/10.1126/science.1147621

Tackley, P. J. (2013). Convection in Io's asthenosphere: Redistribution of nonuniform tidal heating by mean flows. *Journal of Geophysical Research: Planets*, *106*(E12), 32971–32982. https://doi.org/10.1029/2000JE001411

Tackley, P. J., Schubert, G., Glatzmaier, G. A., Schenk, P., Ratcliff, J. T., & Matas, J. P. (2001). Three-dimensional simulations of mantle convection in Io. *Icarus*, *149*(1), 79–93. https://doi.org/10.1006/icar.2000.6536

Tsang, C. C. C., Rathbun, J. A., Spencer, J. R., Hesman, B. E., & Abramov, O. (2014). Io's hot spots in the near-infrared detected by LEISA during the New Horizons flyby. *Journal of Geophysical Research: Planets*, *119*(10), 2222–2238. https://doi.org/10.1002/2014JE004670

Veeder, G. J., Davies, A. G., Matson, D. L., Johnson, T. V., Williams, D. A., & Radebaugh, J. (2015). Io: Heat flow from small volcanic features. *Icarus*, *245*, 379–410. https://doi.org/10.1016/j.icarus.2014.07.028

Zambon, F. (2022). Io hot spots map detected by JUNO/JIRAM images. *Zenodo*. https://doi.org/10.5281/zenodo.7487894

Erratum

In the originally published version of this article, the reference list gave the lead author's name incorrectly as "Davies, A. D.," instead of "Davies, A. G.," in the references Davies (2003), Davies (2007), Davies et al. (2001), and Davies et al. (2007). These references and their citations in text have since been corrected, and the present version may be considered the authoritative version of record.